

Enhancement of Sensitivity-Bandwidth Product of Interferometric GW Detectors using White Light Cavities

M. Salit* and M.S. Shahriar

*Department of Electrical Engineering and Computer Science,
Northwestern University, 2145 Sheridan Rd, Evanston, IL. 60208, USA*

**Corresponding author: m-salit@northwestern.edu*

Abstract: We develop a general model for Michelson-Interferometer based GW detectors that can be easily adapted to include the effects of incorporating a White Light Cavity (WLC) into the design. We show that incorporating a WLC into the design of a detector of the type currently being considered for use in Advanced LIGO yields an enhanced sensitivity which is both higher than what could otherwise be achieved and nearly constant over a bandwidth of at least 63 kHz, encompassing nearly the entire GW spectrum of interest.

PACS Number(s): 42.50.Ct, 42.50.Gy, 42.60.Da

1. Introduction

Astronomers and optical scientists have often worked together to do astronomy, and gravitational wave (GW) astronomy will not be an exception. GW detectors are not optical devices in the sense that telescopes are, but the most promising of them use interferometers to sense gravitational radiation by virtue of its effect on laser light here on earth ¹. This paper deals with the optics of laser interferometric GW detectors. We analyze the frequency response and sensitivity for several potential designs, including a proposed modification that uses a White Light Cavity (WLC) to enhance the sensitivity-bandwidth product. We previously demonstrated a WLC experimentally in rubidium ², and have also explored photorefractive crystals as a potential medium for adapting the technique for use at the working wavelength of LIGO.^{3,4} We review the theory of the WLC and show mathematically the advantages it can offer for LIGO-type GW detectors.

When light travels through a region of space over which a GW is also propagating, the latter causes a periodic variation in the phase of the light field. ⁵ Mathematically, light with this kind of phase modulation may be described as a sum of plane waves of different frequencies. The largest frequency component is the carrier, which is just the frequency of the light when the modulation amplitude is set to zero. The next largest are the two first order sidebands: a Plus-Sideband at the carrier plus the modulation frequency, and a Minus-Sideband at the carrier minus the modulation frequency.⁶ Higher order sideband frequencies exist; however, when the modulation is small, as in the case of GWs, their amplitudes are negligible. The problem of detecting GWs may be reduced to the problem of detecting these sideband frequencies.

The difficulty lies in the fact that the amplitudes of these sideband frequency components are very small, and that they are expected to be separated generally by less than a hundred kilohertz, and in some cases by only tens or hundreds of hertz, from the carrier frequency. These sidebands, then, cannot be separated out from the carrier by means of the usual techniques for filtering light. Prisms and diffraction gratings will not resolve such tiny frequency differences, and even Fabry-Perot cavity filters are less than ideal for this purpose, as they would have to have linewidths down to tens of hertz and very high transmissivity on resonance, so as not to further attenuate the already weak sidebands.

Fortunately we can take advantage of a very convenient property of gravitational radiation: the fact that the modulations it causes along one axis are exactly out of phase with the modulations along a perpendicular axis.⁷ We can therefore use an interferometer to separate out the carrier and the sidebands. Both Michelson and Sagnac interferometers have been proposed for this purpose. We discuss the Sagnac case in reference 8. Here, we will discuss GW detectors that are variations on the Michelson interferometer.

If we arrange the arms of the interferometer along the x and y axes, and the path lengths are chosen correctly, then at one port the carrier light from the x-axis will exactly cancel the carrier light from the y-axis so that we get no carrier frequency light out. The interferometer is on a dark fringe for the carrier. The sidebands, however, having been created by phase modulations with opposite signs, will interfere constructively at this same port.⁶ This means that we can have only the sideband light exiting one port of a Michelson interferometer under the dark fringe condition. Detecting light at that port, in theory, indicates the presence of a GW.

In practice the situation is more complicated. Most of the time light at this dark port only indicates vibrations in the interferometer mirrors or other sources of noise. A great deal of work has been done to minimize noise and to lock the interferometer on a dark fringe condition,⁶ but we would also like to maximize the amplitude of the sideband light falling on the detector. One way of doing that, due to the nature of GWs, is to make the arms of the interferometer very long¹.

Another approach involves the use of optical cavities within the interferometer. If the resonance linewidth of the cavities used is too small, however, then our attempts to use them to enhance the sensitivity of the GW detector will also entail narrowing its linewidth. For this reason, the ideal detector may use a White Light Cavity (WLC), to get the benefits of cavity enhancement described below, without correspondingly narrowing the linewidth of the detector. A WLC is a cavity that resonates over a broader range of frequencies than what its length and finesse would ordinarily entail. The basic theory behind the WLC is discussed in Section 4 below, and explored in greater detail in references 9,10,11 and 12.

The remainder of this paper is organized as follows. Section 2 discusses several GW detector designs that have been proposed, starting from the basic Michelson interferometer configuration. Section 3 gives a general derivation of the frequency response of devices of this type, including those described in the

preceding section. Section 4 discusses the effect of a dispersive medium on that frequency response, and in particular, the effect incorporating WLCs into the design. We conclude in Section 5 with a summary of our results.

2. Variations on the Michelson Interferometer

There are a variety of ways to use cavities to improve the response of the Michelson-interferometer based GW detector. One of the simplest is to add additional mirrors in each arm of the interferometer so as to turn each arm into a Fabry-Perot cavity, as illustrated in Figure 1, below.

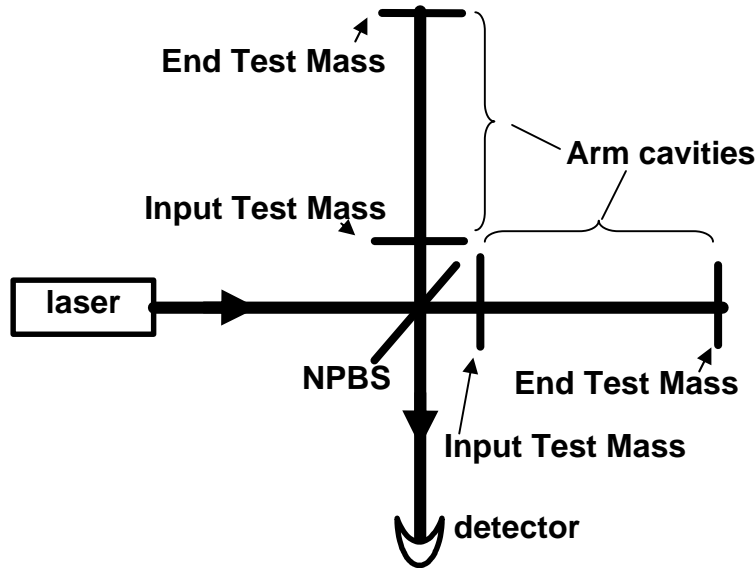


Figure 1: *Michelson interferometer with arm cavities.*

Sideband light is produced from the carrier on each pass as it bounces around the arm cavities. However, though the effect is similar to the use of longer cavity arms, we cannot simply model this as a system with longer effective lengths for the arms. We must take into account the interference effects of multiple bounces within these arm cavities.

We might choose to make the arm cavities resonant for the carrier frequency, for instance. This would allow us to increase the amplitude of the carrier frequency field in the arms by a potentially large factor. Since the sideband field is proportional to the carrier field, the amount of sideband light produced in the arms would then be increased by this same factor. However, the sideband light itself would also undergo multiple reflections within the arm cavities. If the frequency separation between one of the sidebands and the carrier were greater than the resonance linewidth of the cavity, then the multiple reflections of this sideband would interfere destructively. The same conclusion would apply to the other sideband as well, and the signal at the output would be small. Similarly, we might tune the arm cavities to resonate the sidebands, but the carrier would then interfere destructively inside the cavities, making the net signal small.

One way to avoid this trade-off is to place the input mirrors outside the arms of the interferometer, as illustrated in Figure 2, below:

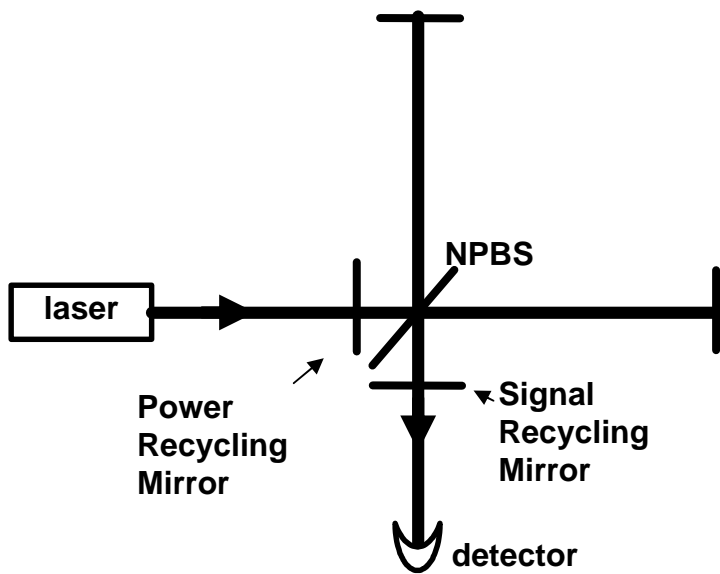


Figure 2: *Michelson Interferometer with dual recycling*

In this configuration, assuming the interferometer is held on the dark fringe condition, the carrier light will only be incident on the mirror labeled Power Recycling Mirror (PRM). It will undergo multiple reflections inside both arms, as if there had been an input mirror in each. Similarly, the sideband frequency light will be reflected back into the arms by the Signal Recycling Mirror (SRM). This Dual Recycling arrangement allows both the carrier and one or both of the sidebands to resonate, within separate but overlapping optical cavities. The disadvantage of this scheme is that the beamsplitter is inside the optical cavity in which the carrier resonates. The current design for Advanced LIGO proposes a circulating power in the arms of 800kW¹³. This amount of power causes thermal distortion and noise on the beamsplitter.

A third option is to combine these two designs, as illustrated in Fig. 3, below.

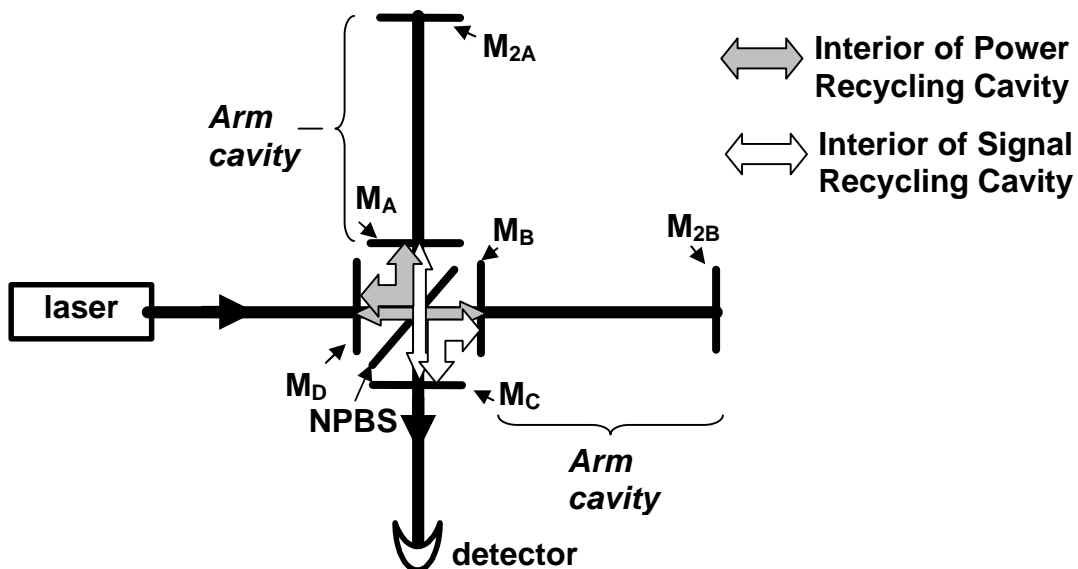


Figure 3: *Michelson Interferometer with dual recycling and arm cavities*

This system, though it comprises many overlapping compound cavities, is not much more difficult to analyze than the simpler version from Fig. 1, under certain conditions. If the two arm cavities are completely identical, with the reflectivity and position relative to the beamsplitter for the mirrors M_A and M_{2A} being exactly the same as those for mirrors M_B and M_{2B} , then we may cease to distinguish between the end test masses M_{2A} and M_{2B} , and refer simply to M_2 .

Likewise, since we have assumed M_A and M_B are identical, we might simply refer to M_{AB} to indicate either one of these input test mass mirrors. Carrier light that is incident on either one from the arms will then travel toward M_D , so long as the interferometer is locked on a dark fringe. Having reflected off of M_D it will then travel back to one of the mirrors M_{AB} , and then back toward M_D again, so that a cavity is formed. We will refer to this cavity as the Power Recycling Cavity (PRC).

The sideband light, likewise, travels from M_{AB} to M_C and back again, so that the sidebands experience a different cavity than the carrier. We will refer to this cavity as the Signal Recycling Cavity (SRC).

In general, any Fabry-Perot cavity may be treated, from the outside, as a mirror that has a frequency dependent reflectivity. Therefore, we treat the PRC, comprising M_{AB} and M_D , as a single compound mirror M_{1CAR} , because it is the compound mirror which reflects the carrier back into the arms. Likewise, we treat the SRC, comprising M_{AB} and M_C , as a single compound mirror M_{1SB} , because it is the compound mirror which reflects the sidebands back into the arms.

The total system may then be modeled as a single Fabry-Perot cavity, with one mirror M_2 having a reflectivity equal to that of the end test masses M_{2A} and M_{2B} , and one mirror M_1 , whose reflectivity is frequency dependent, equal to that of the compound mirror M_{1CAR} for carrier frequency light, and equal to that of the compound mirror M_{1SB} for sideband frequency light. The length of this effective cavity is equal to the distance between M_A and M_{2A} (or equivalently, between M_B and M_{2B}).

The model is illustrated in Fig. 4 below:

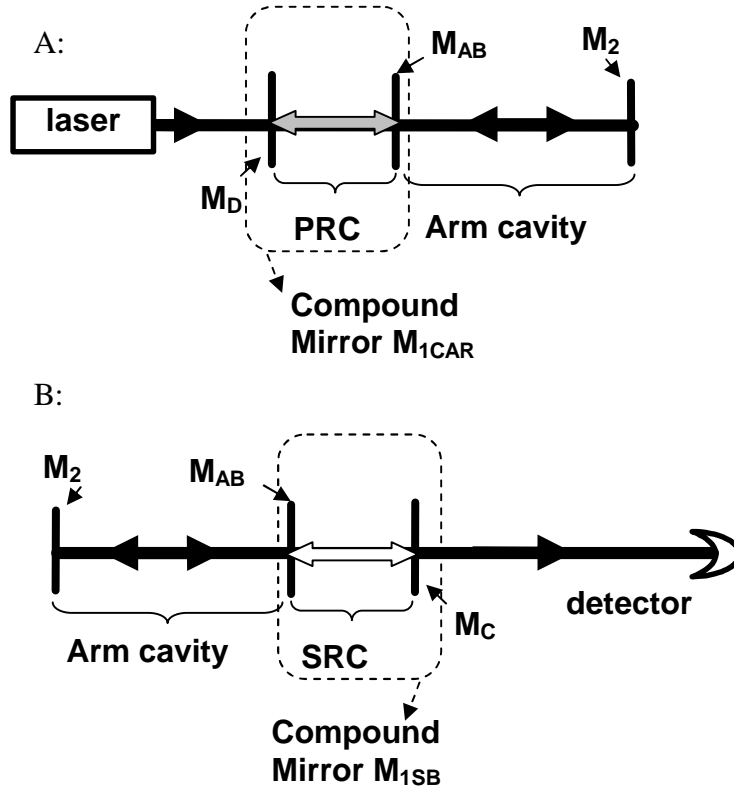


Figure 4: A) Effective path for carrier through system illustrated in Fig. 3 B) Effective path for sideband through system illustrated in Fig. 3

Just as in the case illustrated by Fig. 1, we must choose the length of the arm cavities to resonate either one of the sidebands or the carrier. However, we have the choice, thanks to the fact that we now have tunable compound mirrors, to make the finesse different for the sidebands than for the carrier. The next section analyzes the behavior of this system in mathematical detail. In this section, however, we first summarize the results qualitatively.

There are two different modes of operation for this device. In one, we choose the reflectivity of M_{1CAR} to be high (the PRC is off resonant for the carrier) and choose the length of the arms so that the carrier is resonant in the arm cavities. In this mode, the reflectivity of M_{1SB} must be low, so that the sidebands will be able to transmit out. This is called Resonant Sideband Extraction, since the SRC must be resonant for at least one of the sidebands. This cavity is much shorter than the arm cavities, on the order of 8 m^{14} as opposed to 4000 m, and has a correspondingly broader linewidth – at least 126 kHz even with the highest reflectivity mirror choices we have used in the models in the next section. For realistic choices of mirror reflectivities it is reasonable to treat it as being resonant for both sidebands, and for GW frequencies over the entire spectrum of interest. The amplitude of the signal at the output is increased beyond what we would see in an ordinary Michelson interferometer by the build up of intensity in the carrier field. Since this effect is essentially independent of the GW frequency, we refer to this mode of operation as the broadband mode.

In the other mode, we choose the length of the arms so that at least one of the sidebands is resonant in the arm cavities. Since the carrier will now be off-resonant, we must reduce the reflectivity of M_{1CAR} so that the finesse of the arm cavities, for the carrier, is low enough that it does not destructively interfere. We may, however, increase the reflectivity of M_{1SB} so that the finesse for the resonating sideband is high. Only a small range of sideband frequencies will be able to resonate in the arms however, due to the narrow linewidth of the long, high finesse arm cavities. This means that only sidebands created by a narrow range

of GW frequencies, determined by the arm length we have chosen, are detectable in this mode. For this reason, we refer to this as the narrowband mode. The amount of light falling on the detector is, however, higher in the narrowband mode, when the appropriate GW frequency is present, than it would be in the broadband mode for that same frequency.

Though this system offers better response in both modes than that depicted in Fig. 1, and eliminates many of the heating problems posed by that depicted in Fig.2, it still forces us to choose between high sensitivity and low bandwidth, or high bandwidth and low sensitivity. The WLC proposal that will be described in Section 4 would allow us to have the sensitivity of the narrowband mode over a spectrum as wide as that offered by broadband mode, so that a WLC-enhanced LIGO type interferometer might offer the best of both worlds.

The system depicted in Fig. 3 is also a more general case of those depicted in Fig. 1 and Fig. 2. If we model it mathematically and find its response, we may recover the response for the systems depicted in Fig. 1 and Fig. 2, or for a simple Michelson interferometer with no cavities, by setting the reflectivities of the appropriate mirrors equal to zero. In the next section, we develop this general model.

3. General Model for Michelson-based GW Detectors

B.J. Meers¹⁵ first modeled this system in 1989, but his model is not given in a form that lends itself to the analysis of the effect of a WLC on the system. Furthermore, in the course of developing the model, he makes certain assumptions about mirror reflectivities and resonance conditions which render his final expression less than general, and not directly applicable to two operating modes planned for the Advanced LIGO and described above. We will essentially follow his method in deriving the frequency response of the system illustrated in Fig. 3, but we will adopt a slightly different notation and go beyond the constraints of some of the assumptions he uses.

As Meers did, we will denote the reflectivity of the compound mirror M_{ICAR} by R_{IC} . This is not to be confused with the reflectivity of the mirror labeled M_C , which we will denote simply by R_C . We will denote the reflectivity of the compound mirror M_{ISB} by R_{IS} . Whereas he uses R_{IS} and R_{IC} to denote only the amplitude of the reflectivity, we will allow them to be complex numbers, giving information about both the amplitude and the phase of light reflected off the SRC and PRC, respectively. We can calculate these reflectivities from basic theory of a Fabry-Perot cavity, and keep in mind that they are frequency dependent quantities wherever we use them.

The first step in the derivation is to quantify the effect of a GW on light. Let us choose our coordinates such that the effect of the GW on the metric of space time is described by⁷

$$(1) \quad ds^2 = dx^2(1 + h \cos \mathbf{w}_g t) + dy^2(1 - h \cos \mathbf{w}_g t) + dz^2 - c^2 dt^2$$

Along the path of a light wave, $ds = 0$. Let us assume we have light propagating along the x-axis. Then:

$$(2) \quad \begin{aligned} dx^2(1 + h \cos \mathbf{w}_g t) &= c^2 dt^2 \\ \Rightarrow \frac{dx}{dt} &\approx c \left(1 - \frac{h}{2} \cos \mathbf{w}_g t\right) \end{aligned}$$

The phase the light accumulated as it travels is given by:

$$(3) \quad \begin{aligned} \mathbf{f}_x &= \int_{x_1}^{x_2} k dx = \int_{t-t}^t k \frac{dx}{dt} dt = \int_{t-t}^t kc \left(1 - \frac{h}{2} \cos \mathbf{w}_g t\right) dt \\ \Rightarrow \mathbf{f}_x &= \boxed{\mathbf{w}t - \frac{\mathbf{w}h}{\mathbf{w}_g} \sin\left(\frac{\mathbf{w}_g t}{2}\right) \left(\frac{e^{i\mathbf{w}_g(t-t/2)} + e^{-i\mathbf{w}_g(t-t/2)}}{2}\right)} \end{aligned}$$

The calculation for a beam traveling along the y-axis is identical, except that we use $\frac{dy}{dt} = c(1 + \frac{h}{2} \cos \mathbf{w}_g t)$.

$$(4) \quad \Rightarrow \boxed{\mathbf{f}_y = \mathbf{w}t + \frac{wh}{\mathbf{w}_g} \sin\left(\frac{\mathbf{w}_g t}{2}\right) \left(\frac{e^{i\mathbf{w}_g(t-t/2)} + e^{-i\mathbf{w}_g(t-t/2)}}{2} \right)}$$

Of course $\mathbf{w}t$ is the phase that the light would pick up in the absence of GWs. We define $\mathbf{f}_{prop} = \mathbf{w}t$ as the ordinary propagation phase. In our model, we assume that light traveling along one of the coordinate axes under the influence of GWs picks up a multiplication factor expressed as $e^{i\mathbf{f}_x} = e^{i\mathbf{f}_{prop}} e^{i\mathbf{d}\mathbf{f}_x} \cong e^{i\mathbf{f}_{prop}} (1 + i\mathbf{d}\mathbf{f}_x)$ (where $\mathbf{d}\mathbf{f}_x = \mathbf{f}_x - \mathbf{f}_{prop}$) or as

$$e^{i\mathbf{f}_y} \cong e^{i\mathbf{f}_{prop}} (1 + i\mathbf{d}\mathbf{f}_y) \text{ (where } \mathbf{d}\mathbf{f}_y = \mathbf{f}_y - \mathbf{f}_{prop}\text{).}$$

By using these approximations, we are assuming that the modulation is small enough that the carrier power is effectively undepleted.

First we will consider the amplitude of the carrier field. Let us assume that a field with amplitude E_0 enters through M_{1CAR} , which has a transmissivity T_{1C} and a reflectivity R_{1C} at the carrier frequency. The field, after entering and reflecting off of either arm-end mirror M_2 (which has a reflectivity R_2) returns to the PRC with an amplitude

$$(5) \quad E_1 = E_0 T_{1C} R_2 e^{-2ik_c L} \text{ (where } L \text{ is the length of the arm-end cavity)}$$

This field now reflects off of M_{1CAR} , and then off of M_2 again, returning to the PRC now with an amplitude

$$(6) \quad E_2 = E_0 T_{1C} R_2^2 R_{1C} e^{-4ik_c L}$$

After each reflection thereafter the field picks up the same factor of $R_{1C} R_2 e^{-2ik_c L}$. The steady state field is

the sum $\left(\sum_N E_N \right)$ over all bounces. Therefore in steady state the carrier frequency field inside is

$$(7) \quad E'_{car} = E_0 T_{1C} R_2 e^{-2ik_c L} \sum_{N=1}^{\infty} \left(R_2 R_{1C} e^{-2ik_c L} \right)^{N-1}$$

Again, we have neglected the depletion of the carrier due to the modulation, in this model. Now the sideband fields being continually produced from this steady-state carrier are given, under the approximation described above, by

$$(8) \quad E_{SB} = E'_{car} e^{i\mathbf{w}t} e^{i\mathbf{f}_{prop}} (1 + i\mathbf{b} \left(e^{i\mathbf{w}_g(t-t/2)} + e^{-i\mathbf{w}_g(t-t/2)} \right)) \text{ where } \mathbf{b} = \frac{h\mathbf{w}}{\mathbf{w}_g} \sin(\mathbf{w}_g t / 2)$$

These fields also reflect within the arm-end cavity. Considering only the component at frequency $(\mathbf{w} + \mathbf{w}_g)$, we see that its initial amplitude is

$$(9) \quad E_{+1} = E'_{car} e^{i\mathbf{w}t} e^{-2ik_c L} i\mathbf{b} e^{i\mathbf{w}_g(t-t/2)}$$

Here we have used $\mathbf{f}_{prop} = -2ik_c L$. This field reflects off the SRC and experiences a reflectivity R_{1S} . After another round trip the amplitude is

$$(10) \quad E_{+2} = E'_{car} e^{i\omega t} i\mathbf{b} e^{i\mathbf{w}_g(t-\mathbf{t}/2)} R_{1S} R_2 e^{-2i\left(\frac{\mathbf{w}+\mathbf{w}_g}{c}\right)L_S} e^{-2ik_c L}$$

Note that $(\mathbf{w} + \mathbf{w}_g) / c = k_+$, the wavenumber of the sideband. We have, in this expression, introduced another variable L_S , which is the length of the cavity in which the sidebands are propagating. In the case illustrated by figures 3 and 4, this L_S is the same as L , equal the distance between the end test mass, M_2 , and the input test masses, M_{AB} . However, in the case illustrated by figure 2, these are two distinct numbers, with L_S being equal to the sum of the distance from the end test mass to the beamsplitter and that from the beamsplitter to the signal recycling mirror, and L being equal to the sum of the distance from the end test mass to the beamsplitter and that from the beamsplitter to the power recycling mirror. After n passes, then, the total field is

$$(11) \quad E'_+ = \left(\sum_n E_{+n} \right) = E'_{car} e^{i\omega t} i\mathbf{b} e^{i\mathbf{w}_g(t-\mathbf{t}/2)} \sum_{n=1}^{\infty} R_{1S}^{n-1} R_2^{n-1} e^{-2i(n-1)(\mathbf{w}+\mathbf{w}_g)L_S/c} e^{-2ik_c L}$$

Doing the geometric series sums for E'_{car} and E'_+ , we find that the output field transmitted through the SRC, $E_+ = E'_+ T_{1S}$ is given by

$$(12) \quad \frac{E_+}{E_o e^{i\omega t}} = \frac{T_{1S} T_{1C} R_2}{1 - R_2 R_{1C} e^{-2ik_c L}} \frac{i(h\mathbf{w} / \mathbf{w}_g) \sin(\mathbf{w}_g \mathbf{t} / 2) e^{-2ik_c L} e^{i\mathbf{w}_g(t-\mathbf{t}/2)} e^{-2ik_c L}}{1 - R_{1S} R_2 e^{-2i(\mathbf{w}+\mathbf{w}_g)L_S/c}}$$

The notation here is slightly different from that used by Meers¹⁵, but the result agrees with his provided we define $2L/c = \mathbf{t}$, $\mathbf{d}_c = (-2\mathbf{w}L/c) \bmod 2\mathbf{p}$ and $\mathbf{d}_s = (-2\mathbf{w}L_S/c) \bmod 2\mathbf{p}$. By leaving the expression in terms of the separate wavenumbers of the sidebands and carrier, however, we leave ourselves the option of easily including dispersive effects in this calculation at the next stage.

For the Minus-Sideband, the expression is the same, except with $\mathbf{w}_g \rightarrow -\mathbf{w}_g$, and with R_{1S} potentially taking on a different value, since it is a frequency dependent reflectivity. These amplitudes do not tell us the frequency response of our device directly, however. In practice, the sidebands are detected using a heterodyne scheme, either by allowing a small amount of carrier frequency light to leak through, or by mixing the output signal with carrier frequency light, and detecting the beat signal. To find the total response of the interferometer we need to calculate the amplitude of that beat signal:

$$(13) \quad \mathbf{d}I = E_L E_+^* + E_+ E_L^* + E_L E_-^* + E_- E_L^*$$

Here E_L is the carrier frequency field with which we are mixing our sidebands:

$$(14) \quad E_L = (A / E_0) e^{i(\omega t + \mathbf{f})}$$

In order to do this sum, it is convenient to change our notation slightly. Let $R_{1C} = r_{1C} e^{f_{r1C}}$, and let $R_{1S_+} = r_{1S_+} e^{f_{r1S_+}}$ be the reflectivity of the SRC at the Plus-Sideband frequency, while $R_{1S_-} = r_{1S_-} e^{f_{r1S_-}}$ is the reflectivity of the SRC at the Minus-Sideband frequency. In general, lower case letters for the reflectivity or transmissivity will now be used to denote the magnitude only. We also choose to insert a couple of multiplicative factors equal to one, marked with square brackets. With this convention the equation above may be rewritten as:

(15)

$$\frac{E_+}{E_o e^{i\omega t}} = \frac{t_{1S_+} e^{f_{r1S_+}} t_{1C} e^{if_{r1C}} r_2 i h \omega \sin(\mathbf{w}_g \mathbf{t} / 2) e^{i\mathbf{w}_g (t-\mathbf{t}/2)} e^{-2ik_c L} \left[e^{if_{r1C}} e^{-if_{r1C}} \right] e^{-2ik_c L} \left[e^{if_{r1S_+}} e^{-if_{r1S_+}} \right] \left[e^{-2ik_+ L_S} e^{2ik_+ L_S} \right]}{\mathbf{w}_g \left(1 - r_2 r_{1C} e^{if_{r1C} - 2ik_c L} \right) \left(1 - r_2 r_{1S_+} e^{if_{r1S_+} - 2ik_+ L_S / c} \right)}$$

These additional factors allow us to make use of the identity $\frac{e^{if}}{1 - \mathbf{r}_1 \mathbf{r}_2 e^{if}} = \frac{e^{if} - \mathbf{r}_1 \mathbf{r}_2}{(1 - \mathbf{r}_1 \mathbf{r}_2)^2 (1 + F' \sin^2(f/2))}$, where $F' = \frac{4\mathbf{r}_1 \mathbf{r}_2}{(1 - \mathbf{r}_1 \mathbf{r}_2)^2}$, to write the output in terms of a cavity finesse. We will use F'_C for the finesse of the cavity as experienced by the carrier frequency light, F'_{S_+} for the Plus-Sideband and F'_{S_-} for the Minus-Sideband.

We now have

(16)

$$\frac{E_+}{E_o e^{i\omega t}} = \frac{t_{1S_+} t_{1C} r_2 i h \omega \sin(\mathbf{w}_g \mathbf{t} / 2)}{\mathbf{w}_g} \left(\frac{e^{-2ik_c L + if_{r1C}} - r_2 r_{1C}}{(1 - r_2 r_{1C})^2 \left(1 + F'_C \sin^2\left(\frac{-2k_c L + \mathbf{f}_{r1C}}{2}\right)\right)} \right) \left(\frac{e^{-2ik_+ L + if_{r1S_+}} - r_2 r_{1S_+}}{(1 - r_2 r_{1S_+})^2 \left(1 + F'_{S_+} \sin^2\left(\frac{-2k_+ L_S + \mathbf{f}_{r1S_+}}{2}\right)\right)} \right) \times e^{i\mathbf{w}_g (t-\mathbf{t}/2)} e^{f_{r1S_+}} e^{if_{r1C}} e^{-if_{r1C}} e^{-2ik_c L} e^{-if_{r1S_+}} e^{2ik_+ L_S}$$

We would like to separate out the part of this expression that represents the carrier resonance and the part that represents the sideband resonance. To this end, we define

$$(17) \quad \mathbf{x}_{\pm} = \frac{t_{1C} t_{1S_{\pm}} r_2 h \omega \sin(\mathbf{w}_g \mathbf{t} / 2)}{\mathbf{w}_g (1 - r_2 r_{1C})^2 (1 - r_2 r_{1S_{\pm}})^2}$$

And we let

$$(18) \quad B e^{if_B} = \frac{e^{-2ik_c L + if_{r1C}} - r_2 r_{1C}}{1 + F'_C \sin^2(k_c L - \mathbf{f}_{r1C} / 2)}$$

Now B and \mathbf{f}_B represent the carrier field amplitude and phase in the arm cavities. With this notation,

$$(19) \quad \frac{E_+}{E_0 e^{i\omega t}} = i\mathbf{x}_+ B \left(\frac{1 - r_2 r_{1S_+} e^{2ik_+ L - i\mathbf{f}_{r1S_+}}}{1 + F'_{S_+} \sin^2(k_+ L_S - \mathbf{f}_{r1S_+} / 2)} \right) e^{i\mathbf{w}_g (t-t/2)} e^{i\mathbf{f}_{eff}} e^{i\mathbf{f}_{r1S_+}} e^{i\mathbf{f}_B}$$

where $\mathbf{f}_{eff} = \mathbf{f}_{r1C} - \mathbf{f}_{r1C} - 2ik_C L$

With this expression and some trigonometric identities, it is now relatively straightforward to calculate the total response of our device. In keeping track of the phase of the carrier, it proves convenient to define $\mathbf{f}_{net} = (\mathbf{f}_{eff} - \mathbf{f} + \mathbf{f}_B)$. We also replace t with $2L/c$ at this point so as to make all length dependence explicit.

We find that

(20)

$$E_+ E_L^* + E_+^* E_L = \frac{-2AB\mathbf{x}_+}{1 + F'_{S_+} \sin^2(k_+ L_S - \mathbf{f}_{r1S_+} / 2)} \times \left[\sin \left(\mathbf{w}_g \left(t - \frac{L}{c} \right) + \mathbf{f}_{r1S_+} + \mathbf{f}_{net} \right) - r_2 r_{1S_+} \sin \left(\mathbf{w}_g \left(t - \frac{L}{c} \right) + \mathbf{f}_{r1S_+} + \mathbf{f}_{net} + 2k_+ L_S - \mathbf{f}_{r1S_+} \right) \right]$$

Finally, we choose

$$(21) \quad \mathbf{f}_C = \mathbf{f}_{net} - \mathbf{p} / 2 = \mathbf{f}_{r1C} - \mathbf{f}_{r1C} - 2k_C L - \mathbf{f} + \mathbf{f}_B - \mathbf{p} / 2$$

This variable keeps track of the total phase of the carrier, and the term $\mathbf{p} / 2$ allows us turn our sine functions into cosine functions. Note that the unsubscripted \mathbf{f} comes from assuming our sidebands were beating with a carrier frequency field of the form $E_L = (A/E_0) e^{i(\omega t + \mathbf{f})}$. We will assume that this phase is controllable, and that we can always choose it so that the output is optimum. The signal from our device is then

(22)

$$\begin{aligned}
\mathbf{d}I &= E_L E_+^* + E_+ E_L^* + E_L E_-^* + E_- E_L^* \\
&= 2AB \left[\left(\frac{\mathbf{x}_+ \cos(\mathbf{w}_g(t-L/c))}{1 + F'_{S_+} \sin^2(k_+ L_S - \mathbf{f}_{r_{1S_+}}/2)} \right) \left(r_2 r_{1S_+} \cos(2k_+ L - \mathbf{f}_{r_{1S_+}} + \mathbf{f}_{r_{1S_+}} + \mathbf{f}_C) - \cos(t_{1S_+} + \mathbf{f}_C) \right) \right. \\
&\quad + \left(\frac{\mathbf{x}_+ \sin(\mathbf{w}_g(t-L/c))}{1 + F'_{S_+} \sin^2(k_+ L_S - \mathbf{f}_{r_{1S_+}}/2)} \right) \left(-r_2 r_{1S_+} \sin(2k_+ L - \mathbf{f}_{r_{1S_+}} + \mathbf{f}_{r_{1S_+}} + \mathbf{f}_C) + \sin(t_{1S_+} + \mathbf{f}_C) \right) \\
&\quad + \left(\frac{\mathbf{x}_- \cos(\mathbf{w}_g(t-L/c))}{1 + F'_{S_-} \sin^2(k_- L_S - \mathbf{f}_{r_{1S_-}}/2)} \right) \left(r_2 r_{1S_-} \cos(2k_- L - \mathbf{f}_{r_{1S_-}} + \mathbf{f}_{r_{1S_-}} + \mathbf{f}_C) - \cos(t_{1S_-} - \mathbf{f}_C) \right) \\
&\quad \left. + \left(\frac{\mathbf{x}_- \sin(\mathbf{w}_g(t-L/c))}{1 + F'_{S_-} \sin^2(k_- L_S - \mathbf{f}_{r_{1S_-}}/2)} \right) \left(r_2 r_{1S_-} \sin(2k_- L - \mathbf{f}_{r_{1S_-}} + \mathbf{f}_{r_{1S_-}} + \mathbf{f}_C) - \sin(t_{1S_-} + \mathbf{f}_C) \right) \right] \\
&\equiv P \cos(\mathbf{w}_g(t-L/c)) + Q \sin(\mathbf{w}_g(t-L/c))
\end{aligned}$$

To find the magnitude of this signal, then, we have only to add the amplitudes of the sine and cosine terms in quadrature.

$$(23) \quad |\mathbf{d}I| = \sqrt{P^2 + Q^2}$$

This rather complicated expression gives the full response of the system illustrated in figure 3, if we set $L_S = L$. In the limit where $r_{1S_+} = r_{1S_-} = r_{1C}$, this also gives the response of the simpler system illustrated in figure 1. Finally, this expression can give us the response of the system illustrated in Fig. 2 as well, where $L_S \neq L$, $r_{1S_{\pm}}$ is equal to the reflectivity of the SRM, and, r_{1C} is equal to that of the PRM.

A GW detector, in the configuration illustrated in Fig. 3 and described by the above equation, has two basic modes of operation, as previously discussed. In the narrowband mode, the SRC is tuned to be far off resonance for the sidebands, so that the reflectivity of the SRC is high, and therefore the finesse of the arm cavities is high for the sidebands. A length is chosen for the arm cavities so that a sideband of a corresponding wavelength will resonate. The PRC is tuned to near resonance for the carrier, so that the finesse of the arm cavity for the carrier is low enough to prevent destructive interference from reducing the carrier amplitude. In the broadband mode, the SRC is tuned to be near resonant so that its transmission is high, and its reflectivity low. The arm length is chosen so that the carrier will resonate, and the finesse of the arm cavities for the carrier is made large by tuning the PRC far off resonance.

Below, the response for the two cases, calculated using the equation above, is plotted. We have also plotted, as Figure 5c, what the narrowband response would look like if the carrier could, in some way, be kept on resonance in the arm end cavity even as one of the sidebands resonates as well. Alternatively, this is the response that would be achieved if the power in the laser could simply be turned up to compensate for the fact that the carrier is not resonant in the arms.

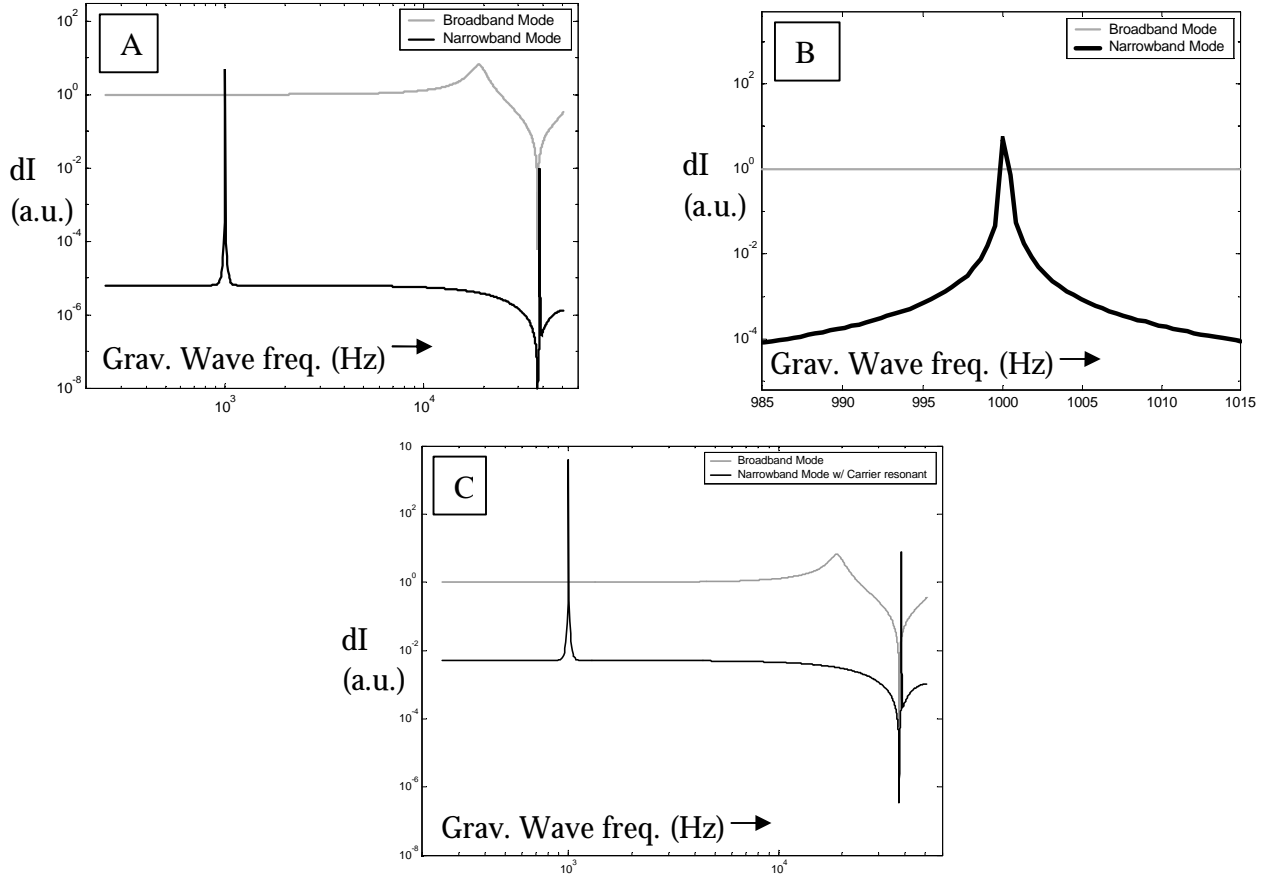


Figure 5: A) Signal output as a function of gravitational frequency for a GW detector of the type illustrated in Fig. 3, in the two different modes, over the range of GW frequencies of interest. B) Detail of plot presented in part A showing linewidth of the narrowband mode peak. C) Shows response if carrier is artificially kept resonant even in narrowband mode. See text for details.

The values presented in the table below were used in calculating the response.

Table 1: Values used in plotting Fig. 5

$c=3*10^8$
$w=2*\pi*c/(1064*10^{(-9)})$
$h=10^{-12}$
$r_2=1$
$t_{AB}=\text{sqrt}(.005)$
$r_{AB}=\text{sqrt}(1-.005)$
$r_D=\text{sqrt}(1-.06)$
$t_D=\text{sqrt}(.06)$
$r_{1cLRC}=\text{abs}(t_{AB}^2*r_D*\exp(-.9999*2*i*\pi)/(1-r_D*r_{AB}*\exp(-.9999*2*i*\pi))-r_{AB})$
$t_{1cLRC}=\text{abs}(t_{AB}^2*t_D*\exp(-.9999*2*i*\pi)/(1-r_D*r_{AB}*\exp(-.9999*2*i*\pi)))$
$r_{1cHRC}=\text{abs}(-t_{AB}^2*r_D/(1+r_D*r_{AB})-r_{AB})$
$t_{1cHRC}=\text{abs}(-i*t_{AB}^2*t_D/(1+r_D*r_{AB}))$
$r_C=\text{sqrt}(1-.05)$
$t_C=\text{sqrt}(.05)$
$r_{Cnb}=\text{sqrt}(1-.002)$
$t_{Cnb}=\text{sqrt}(.002)$
$L_{1SLR}=2*\pi*1.565*10^7/(2*(kc+2*\pi*1000/c))$

$$\begin{aligned}
L1_{SHR} &= \pi(3.13 \times 10^7 + 1) / (2(\kappa + 2\pi \times 1000/c)) \\
A &= 100/334 \\
\phi_C &= \pi/3 \\
L_{BB} &= (2\pi \times 37594 \times 10^{10}) / \kappa \\
L_{NB} &= \frac{(0.75188\pi \times 10^{10}) + 5 \times \text{angle}(t_{AB}^2 r_C \exp(-2i(w + 2\pi \times 1000)L1_{SHR}/c))}{(1 - r_C r_{AB} \exp(-2i(w + 2\pi \times 1000)L1_{SHR}/c) - r_{AB})} (\kappa + 2\pi \times 1000/c)
\end{aligned}$$

In these graphs, a variable q_+ represents the propagation phase picked up by the Plus-Sideband in traveling from one end of the arm to the other, so that $2q_+$ is the round-trip propagation phase in the arms. Here q_+ is chosen to run between $0.48P$ and $1.82P$, for the larger scale graph, or $0.46P$ and $0.54P$ for the smaller scale. The GW frequency on the x-axis is derived from q_+ using $f_g = ((c/L_{NB})(q_+ + 2P \times 3759400000) - w) / 2P$, and the quantity q_- , representing the propagation phase of the Minus-Sideband, is also derived from it using $q_- = q_+ - 2 \times (2P f_g) / c$. Both h , the amplitude of the GW, and A , the amplitude of the heterodyning beam, represent arbitrary scale factors in these equations, appearing only as multiplicative constants. The graph has been scaled so that the broadband response at low frequency is equal to one.

The variables r_2 , r_{AB} , t_{AB} , r_C , t_C , r_D , and t_D , represent the reflectivity and transmissivity of the mirrors labeled M_2 , M_{AB} , M_C and M_D , respectively, in Figs. 3 and 4. These values are taken from reference 13, and are the currently planned values for the Advanced LIGO system. The variables r_{Cnb} and t_{Cnb} represent the different reflectivity and transmissivity that might be chosen for M_C if the interferometer were to be operated in the narrowband mode. The variables $r1_{LRC}$ and $t1_{LRC}$ represent the reflectivity and transmissivity of the PRC when it is tuned almost to resonance – these values are used in plotting the narrowband response. Because r_{AB} is not equal to r_D , it is not possible to reduce this reflectivity to zero. However it is not necessary for the PRC reflectivity to be equal to zero in the narrowband mode, only that it be low enough to reduce the finesse of the arm cavities to the point that the linewidth of the arms becomes sufficiently broad to include the carrier. LRC stands for Low Reflectivity for Carrier. By the same token, HRC stands for High Reflectivity for Carrier and $r1_{CHRC}$ and $t1_{CHRC}$ represent the reflectivity and transmissivity of the PRC when it is tuned exactly half way between two resonance peaks, so that the reflectivity of the PRC is maximized. These are the values that are used in plotting the broadband response.

Similarly, $L1_{SLR}$ and $L1_{SHR}$ represent two different choices for the length of the SRC. The reflectivity of the SRC is calculated from standard Fabry-Perot theory using one of these two values for the length of the cavity. When $L1_{SLR}$ is used, the SRC is on resonance for the Plus-Sideband due to a GW at a frequency of 1 kHz. Again, the SRC cannot be 100% transmitting due to the mismatch in r_{AB} and r_C . The fact that the sidebands are to some extent still resonating in the arms even in the broadband mode accounts for the peak that occurs at higher frequencies in the broadband mode graph. Note that since the length of the cavity is fixed by the requirement that the carrier resonate, the frequency at which this peak occurs is not tunable, unlike the frequency of the narrowband peak. The transmissivity of the SRC, though not one, is nevertheless maximized in these broadband mode plots. When the length $L1_{SHR}$ is plugged into this expression instead, then a sideband due to a 1 kHz GW becomes off resonant in the SRC, exactly half way between two peaks. With this choice of length, the SRC becomes highly reflective over all frequencies of interest. Both lengths evaluate to approximately 8.32 m, close to the proposed length of the SRC for the Advanced Ligo¹⁴. In these plots, no approximations are used for calculating the reflectivity of the SRC. The full expression from Fabry-Perot theory is used to calculate a the reflectivity at each frequency within the plot range and separately for both sidebands. Finally, L_{BB} is the length of the arm cavity in broadband mode, resonant for the carrier, and L_{NB} is that used for narrowband mode, resonant for the Plus-Sideband due to a GW at 1 kHz.

The fall-off near 40kHz which is common to all of the modes of operation is a result of the $(1/w_g) \sin(w_g t / 2)$ term which appears as an overall multiplicative factor in the frequency response expression, and which goes to zero at $f_g = 1/t \approx 37.5 \text{ kHz}$.

Clearly hybrid modes of operation exist, with different choices for the lengths of the SRC and PRC and different choices for the phase of the carrier frequency beam with which the sidebands beat, but these two cases are enough to give a general idea of the behavior in broadband mode vs. narrowband mode using the Advanced LIGO parameters.

4. Dispersive Effects

Having written the output of the device in terms of the sideband wavenumbers k_+ and k_- , we are now in a position to include easily the effects of dispersion on the system. The effect of the medium is to change the wavelength of light within it, so that $\mathbf{l}_{medium} = \mathbf{l}_{vacuum} / n$, where n is the index of refraction of the medium. Equivalently, we may multiply the wavenumber by n , i.e. $k_{medium} = n k_{vacuum}$.

If we had a Fabry-Perot cavity of length L , the propagation phase light would ordinarily pick up on traveling from one end to the other is

$$(24) \quad \mathbf{q}_{vacuum} = kL \text{ (where } k = k_{vacuum} \text{)}$$

If, however, we assume a cavity of length L partially filled by a medium of length l , that phase becomes

$$(25) \quad \mathbf{q} = k(L-l) + n(\mathbf{w})kl$$

The phase picked up by light making one round trip in the cavity is then

$$(26) \quad \mathbf{q}_{r.t.} = 2k(L-l) + 2n(\mathbf{w})kl$$

Assuming the light does not pick up any additional phase shifts as it propagates, the resonance condition is

$$(27) \quad \mathbf{q}_{r.t.} = 2\mathbf{p}m \text{ (for integer } m \text{)}$$

If the light does pick up some phase shift, e.g. by reflecting off of a phase shifting mirror, then the resonance condition is altered so that the total phase picked up is equal to $2\mathbf{p}m$, and the round trip propagation phase is equal to $2\mathbf{p}m$ minus the extra phase due to the reflection.

In either case, resonance requires that the round trip phase $\mathbf{q}_{r.t.}$ be equal to some predetermined constant. In free space, there would be only one value of \mathbf{w} which would fulfill the resonance condition. In a medium, however, we may have $\mathbf{q}_{r.t.}$ depend on \mathbf{w} in a non-linear way. If we require that

$$(28) \quad \left. \frac{d\mathbf{q}_{r.t.}}{d\mathbf{w}} \right|_{\mathbf{w}_0} = 0$$

at some frequency \mathbf{w}_0 , then the round trip phase will not change with frequency at all for very small deviations from \mathbf{w}_0 , and will change by very small amounts for some range of frequencies around \mathbf{w}_0 . If \mathbf{w}_0 happens to be the resonant frequency of the cavity, then a range of frequencies around \mathbf{w}_0 will also be very close to resonance. The key to making a WLC is to make this range sufficiently large that the cavity resonates over a much wider bandwidth than it would if it were empty.

Substituting $k = \mathbf{w}/c$ into equation 26 (since k here is the vacuum wavenumber), and taking the derivative, we find

$$(29) \quad \left. \frac{d\mathbf{q}_{r.t.}}{d\mathbf{w}} \right|_{\mathbf{w}_0} = \left[\frac{d}{d\mathbf{w}} \left(2 \frac{\mathbf{w}}{c} (L-l) + 2 n(\mathbf{w}) \frac{\mathbf{w}}{c} l \right) \right]_{\mathbf{w}_0}$$

$$\approx 2 \left(\frac{L}{c} + \left. \frac{dn}{d\mathbf{w}} \right|_{\mathbf{w}_0} \frac{\mathbf{w}_0}{c} l \right) \quad (\text{if } n(\mathbf{w}_0) \approx 1)$$

Therefore the condition $\left. \frac{d\mathbf{q}_{r.t.}}{d\mathbf{w}} \right|_{\mathbf{w}_0} = 0$ requires that

$$(30) \quad \left. \frac{dn}{d\mathbf{w}} \right|_{\mathbf{w}_0} = \frac{-L}{l} \frac{1}{\mathbf{w}_0}$$

The simplest model for a WLC assumes an index of refraction which is linear \mathbf{w} and has a slope given by the equation above:

$$(31) \quad n(\mathbf{w}) = \frac{-L}{l} \frac{1}{\mathbf{w}_0} (\mathbf{w} - \mathbf{w}_0)$$

More complete models might assume $n(\mathbf{w})$ has the lineshape of the derivative of a Lorentzian, and choose the coefficients in the equation for this lineshape to give the appropriate slope at the center, or even more realistically, reproduce the lineshape of an index due to double gain peaks ², for example, again with coefficients chosen such that the index has the appropriate slope between the two peaks.

Whichever functional form of $n(\mathbf{w})$ we choose, we may plug it into equation 25 to find its effect on the phase of light propagating through the cavity. The linear form of $n(\mathbf{w})$, for instance, gives

$$(32) \quad \mathbf{q} = k(L-l) + \frac{-L}{l} \frac{1}{\mathbf{w}_0} (\mathbf{w} - \mathbf{w}_0) (kl)$$

$$= k(L-l) + \frac{-L}{k_0} (k - k_0) (k)$$

where $k_0 = \mathbf{w}_0/c$ and k is the vacuum wavenumber. All standard Fabry-Perot cavity analysis still applies, provided we use this expression for the propagation phase of light traveling from one end to the other of the cavity.

From this, we see that in order to find the effect of changing the arm cavities into WLCs, on a LIGO type GW detector, we need only make the following substitutions:

$$\begin{aligned}
k_+ L_S &\rightarrow k_+ (L_S - l) + \frac{-L_S}{k_0} (k_+ - k_0) (k_+) \\
(33) \quad k_- L_S &\rightarrow k_- (L_S - l) + \frac{-L_S}{k_0} (k_- - k_0) (k_-) \\
k_c L_S &\rightarrow k_c (L_S - l) + \frac{-L_S}{k_0} (k_c - k_0) (k_c)
\end{aligned}$$

Note that these expressions imply that we are placing the medium in the cavity of length L_S . In the type of system illustrated in Fig. 3, where $L_S = L$, this means the medium must be placed in the arms of the interferometer. In the case illustrated by Fig. 2, however, the medium may be placed between the beamsplitter and the Signal Recycling Mirror. In any case, we want to place it in whatever cavity stores the sidebands and has a length on the order of 4 km, in order to broaden the ordinarily very narrow linewidth associated with such a long resonator.

In the expressions above, we have used the linear form of $n(\omega)$. Using more realistic functional forms of $n(\omega)$ will, of course, give a more realistic analysis of the behavior of the system, but all of the appropriate models for the index are linear over at least some range of frequencies, and over that linear bandwidth of the index, this is a good approximation. In our experimental demonstrations of the WLC¹⁰, we have seen a linear bandwidth approximately 5 MHz which is considerably broader than the GW bandwidth of interest, 0 to 50 KHz.

Making these replacements and then replotting the results for narrowband and broadband mode, we get Figure 6 A. We have also included, as Figure 6 B, a plot of what the frequency response would look like if the carrier could be kept resonant (or the laser power turned up to compensate for the lack of resonant build up) even in the narrowband mode. Note that in this case the Narrowband Mode graph reaches almost to the level of the Narrowband Mode with WLC graph. One might expect the two graphs to have the same value at the resonant frequency of 1 kHz. Instead, the WLC response is twice as big as the narrowband response even if the carrier is artificially made resonant. This is because in the WLC, both sidebands resonate instead of just one.

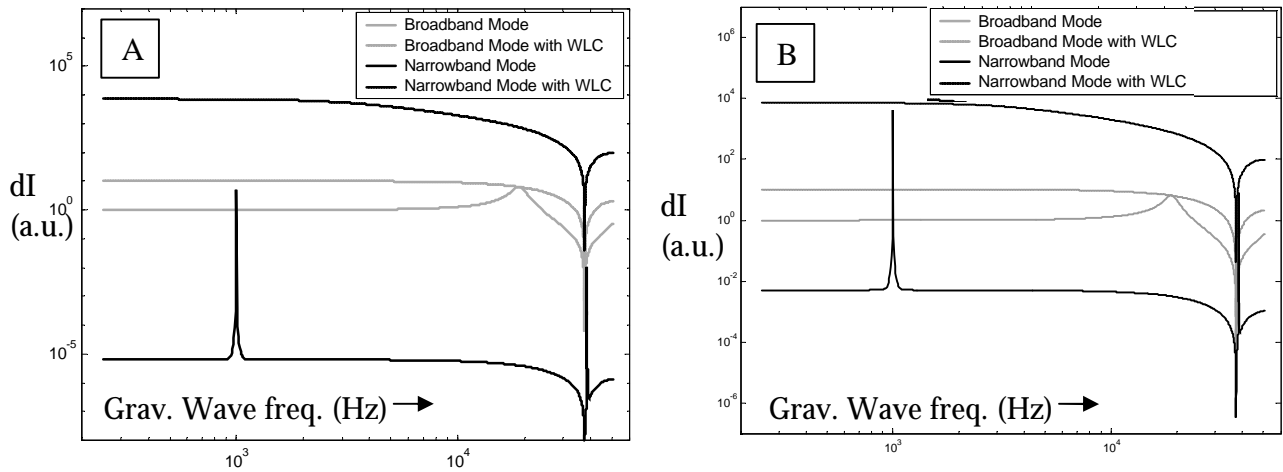


Figure 6: A) Frequency response of a GW detector of the type illustrated in Fig. 3 with and without WLC, in broadband and narrowband mode. B) Same as A but with carrier artificially kept resonant even in narrowband mode See text for details.

The WLC response is not only significantly broader than the narrowband response, but significantly higher as well. This is because, unlike in the empty cavity case where we had to choose between resonating one of the sidebands (narrowband mode) and the carrier (broadband mode), with the WLC we may resonate the carrier and both sidebands. There is no trade-off.

The cases illustrated above are for the Advance LIGO type detector illustrated in Fig. 3. We have also carried out the derivation, and developed the frequency response graph, for the type of detector illustrated in Fig. 2, with and without a WLC. In this case, the possibility of independently varying the length of the cavity for the sidebands and for the carrier means that the trade-off between sideband resonance and carrier resonance is not an issue. Both may resonate even without a WLC. However there is still a narrowband mode. When the SRM is absent, the sidebands do not resonate at all and the signal level is determined by the intensity of the carrier field only, and depends on the GW frequency only through the $(1/\omega_g)\sin(\omega_g t/2)$ factor. When the SRM is present, however, the destructive interference of non-resonant sidebands in the cavity formed by the SRM and the end test masses can drop the signal level effectively to zero no matter how strongly the carrier is resonating in its cavity. On the other hand, the constructive interference of resonant sidebands will cause an increase in the signal level over the case with no SRM, by a factor equal to the one by which the sideband field intensity in the arms is increased on resonance. The result is that, in the presence of an SRM, the response is narrowband and similar to that illustrated in Fig. 5C and 6B. In this case, it is simple to allow the carrier to resonate along with one of the sidebands, in the narrowband mode. Incorporating a WLC again gives a broadband response equal to twice the peak value of the narrowband response, since with the WLC, both sidebands will resonate along with the carrier. This is illustrated in figure 7. In this case, it is worth noting that increasing the reflectivity of the SRM increases the sensitivity of the detector without compromising the bandwidth, so that with the incorporation of a WLC, a detector of this type can be made far more sensitive, for a given carrier power, than would be feasible without the WLC.

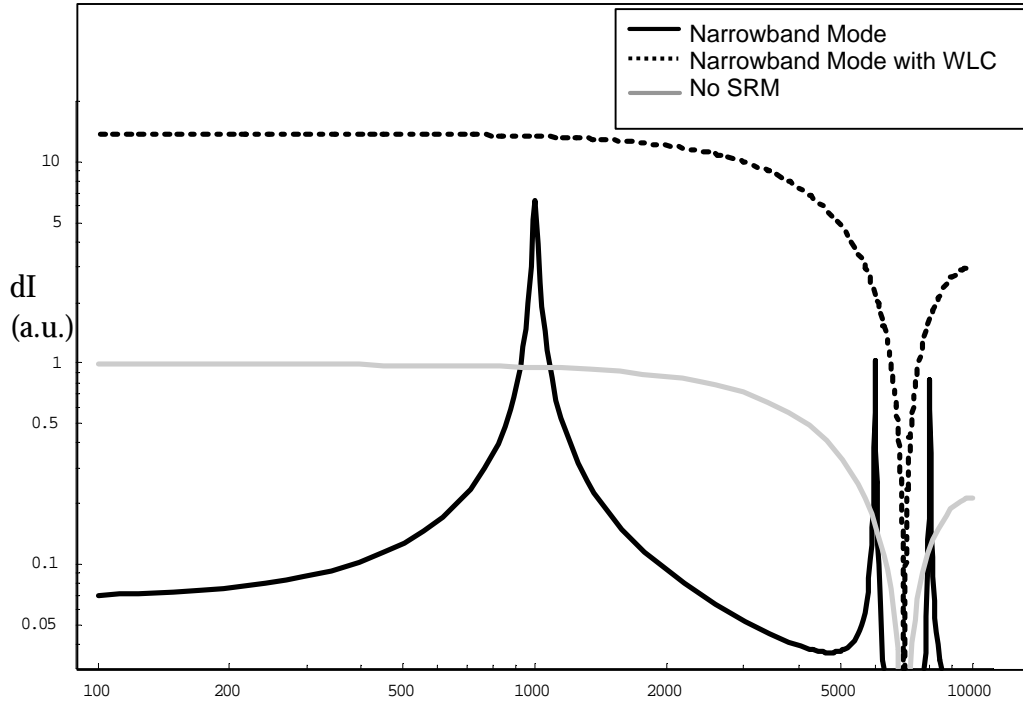


Figure 7: Response for the type of system illustrated in Fig. 2 with SRM reflectivity of $\sqrt{.98}$, other parameters chosen to match those used in ref. 15

Note that the broader linewidth of the narrowband mode in this case is due to the fact that the reflectivity in the narrowband mode is no higher than that of the SRM itself, whereas in the design previously discussed, the relevant reflectivity is that of the signal recycling cavity. As discussed in reference 8, this simpler type of design may in fact be more suitable for use with a WLC than the design illustrated by Fig. 3. In this configuration, illustrated by Fig. 2, the dispersive medium may be placed outside of the interferometer arms, between the beamsplitter and the signal recycling mirror. In this case, the beam power within the medium can be smaller, since the high power carrier is not incident on the medium in this configuration. The design illustrated by figure 2 also requires a simpler control system, with fewer cavities to lock. It does suffer from the issues regarding the heating of the beamsplitter as described earlier, and is slightly less flexible. One other option, discussed in 16, is to add yet another mirror to the design illustrated in Figure 2, between the signal recycling mirror and the detector. This would yield some of the same flexibility as those offered by the design illustrated in Figure 3, in that the sidebands would again reflect off of a compound output coupler, the reflectivity of which can be tuned to give whatever finesse we choose for the cavity which stores the sidebands in the arms, while still allowing both a sideband and the carrier to resonate in the arms.

The analysis in this paper can easily be extended to cover this case by setting R_C equal to the reflectivity of a cavity. Alternative designs¹⁷ using other optical systems to vary the reflectivity of the SRM can be treated in the same way. It is not our purpose here to argue for one design or another, but rather to present a general analysis which can be used to describe the frequency response, and the effect of a WLC on it, for any variation on the basic Michelson design. We have also proposed a design incorporating the WLC into a Sagnac interferometer⁸. We believe that any of these designs can benefit from the incorporation of a workable WLC.

5. Conclusion

Almost all Michelson-based GW detectors can be described by equation 22 of this document. This equation follows from basic Fabry-Perot theory, provided the arms of the interferometer are identical, and involves treating some pairs of mirrors as a single compound mirror with a frequency dependent reflectivity, in certain cases.

The effect of introducing a medium into such a system is to change the propagation phase of the light within the long arm cavities. If the medium has a negative dispersion with a slope given by equation 30, that propagation phase will not vary with frequency over some range, and the resonance bandwidth of the cavity will be broadened. This will have the effect, for all of the variations on the Michelson interferometer that we have discussed, of both broadening the bandwidth of the detector and increasing its sensitivity to some degree by preventing destructive interference within the cavity.

The method given here for calculating the effect of a WLC on any Michelson-based GW detector allows us to consider a variety of different designs, each with its own advantages and disadvantages. The graph shown in Fig. 6 shows that a WLC could significantly improve a GW detector based on the design currently proposed for Advanced LIGO.

The potential benefits of a WLC are great enough that we believe the possibility should be a factor in future design discussions, and we have tried here to provide the tools necessary for evaluating those designs.

-
- ¹ J. Hough, B.J. Meers, G.P. Newton, N.A. Robertson, H. Ward, B.F. Schutz, I.F. Corbett, and R.W.P. Drever, "Gravitational Wave Astronomy -- Potential and Possible Realisation", *Vistas in Astronomy* **30**, 109 (1987)
- ² G. S. Pati, M. Salit, K. Salit, and M. S. Shahriar, "Demonstration of a Tunable-Bandwidth White-Light Interferometer Using Anomalous Dispersion in Atomic Vapor", *Phys. Rev. Lett* **99**, 133601 (2007)
- ³ H.N. Yum, M. Salit, G.S. Pati, S. Tseng, P.R. Hemmer, M.S.Shahriar, "Fast-Light in a Photorefractive Crystal for Gravitational Wave Detection" submitted to *Optics Express*, <http://arxiv.org/abs/0809.3913>
- ⁴ Q. Sun, M. S. Shahriar, M. S. Zubairy, "Slow light and fast light in a photorefractive crystal", <http://lapt.eecs.northwestern.edu/preprints/slow-fast-prc.pdf>
- ⁵ F.I. Cooperstock and V Faraoni, "Laser-Interferometric Detectors of Gravitational Waves", *Class. Quantum Grav.* **10**, 1189, (1993)
- ⁶ E.D. Black, R. N. Gutenkunst, "An introduction to signal extraction in interferometric Gravitational Wave detectors", *Am. J. Phys.* **71**, 365 (2003).
- ⁷ J.B. Hartle, *Gravity: An Introduction to Einstein's General Relativity*, Addison Wesley, San Francisco, (2003)
- ⁸ M.S. Shahriar and M. Salit, "Application of Fast Light in Gravitational Wave Detection with Interferometers and Resonators," *Journal of Modern Optics* (to be published) <http://lapt.ece.northwestern.edu/preprints/FastLightInGWDetection.pdf>
- ⁹ R.H. Rinkleff, A. Wicht, "The concept of White Light Cavities Using Atomic Phase Coherence", *Physica Scripta* **T118**, 85 (2005).
- ¹⁰ M. Salit, G. S. Pati, K. Salit, and M. S. Shahriar, 'Fast-light for astrophysics: super-sensitive gyroscopes and Gravitational Wave detectors', *Journal of Modern Optics* **54** , 2425 (2007).
- ¹¹ S. Wise, G. Mueller, D. Reitze, D.B. Tanner, B.F. Whiting, "Linewidth-broadened Fabry–Perot cavities within future Gravitational Wave detectors", *Class. Quant. Grav.* **21**, S1031 (2004).
- ¹² S. Wise, V. Quetschke, A. J. Deshpande, G. Mueller, D.H. Reitze, D. B. Tanner, B. F. Whiting, Y. Chen, A. Tunnermann, E. Kley, T. Clausnitzer, "Phase effects in the diffraction of light: Beyond the grating equation", *Phys. Rev. Lett.* **95**, 013901 (2005).
- ¹³ LIGO Laboratory / LIGO Scientific Collaboration, "Advanced LIGO Reference Design: LIGO-060056-08-M", <http://www.ligo.caltech.edu/docs/M/M060056-08/M060056-08.pdf> , 23 May 2007
- ¹⁴ Y. Pan, "Optimal degeneracy for the signal-recycling cavity in advanced LIGO," <http://arxiv.org/PS/cache/gr-qc/pdf/0608/0608128v1.pdf>
- ¹⁵ B.J. Meers, "The Frequency Response of Interferometric Gravitational Wave Detectors", *Physics Letters A* **142**, 465, (1989)
- ¹⁶ B. J. Meers and K. A. Strain, "Wave-front Distortion in Laser-interferometric Gravitational-wave Detectors", *Phys. Rev. D* **43**, 3117 (1988).

¹⁷ Gl. de Vine, D. A. Shaddock, and D. E. McClelland, "Experimental demonstration of variable-reflectivity signal recycling for interferometric gravitational-wave detectors", *Optics Letter* **27**, 1507 (2002)